arXiv:1601.00915v2 [cond-mat.mes-hall] 21 Jan 2016

Superlattice gain in positive differential conductivity region

David O. Winge,[1,*] Martin Franckié,[1] and Andreas Wacker[1]

[1] *Mathematical Physics, Lund University, Box 118, 22100 Lund, Sweden*

(Dated: January 22, 2016)

We analyze theoretically a superlattice structure proposed by A. Andronov et al. [JETP Lett 102, 207 (2015)] to give Terahertz gain for an operation point with positive differential conductivity. Here we confirm the existence of gain and show that an optimized structure displays gain above 20 cm^{-1} at low temperatures, so that lasing may be observable. Comparing a variety of simulations, this gain is found to be strongly affected by elastic scattering. It is shown that the dephasing modifies the nature of the relevant states, so that the common analysis based on Wannier-Stark states is not reliable for a quantitative description of the gain in structures with extremely diagonal transitions.

PACS numbers: 72.10.-d, 72.20.-i

Semiconductor superlattices[1] (SLs) had always been considered as an interesting candidate for THz gain materials due to the Bloch gain[2], which was finally experimentally confirmed more than 30 years later[3–5]. However, this type of gain is intrinsically connected with the negative differential conductivity in the current-field relation, so that the formation of field domains[6–9] strongly limits its observation and practical use. As an alternative, it was suggested[10] that gain can be present in the positive differential conductivity region of SLs where resonant tunneling over several barriers[11–13] is relevant. The idea is to operate the SL slightly below the tunneling resonance from the ground state of well μ to the excited state in the next-neighboring well $\mu + 2$ (see the inset of FIG. 1), which guarantees positive differential conductivity. At the same time, gain is suggested for the strongly diagonal transition to the excited state in the well $\mu + 3$, which is actually lower in energy than the ground state in well μ. More detailed experimental studies confirmed the suggested shape of the current-field relation, but were not conclusive with respect to THz gain[14]. Thus the question remains, whether this type of gain exists at all and whether it is strong enough to overcome losses. In order to address this question, we performed detailed simulations with our non-equilibrium Green's function (NEGF) simulation scheme[15], which are reported here. We find that this particular gain mechanism exists, but that it is not particularly strong for the structure proposed. Testing different doping densities and layer sequences, we observe gain above 20/cm at low temperatures, which could overcome losses in typical THz waveguides[16]. We noticed that dephasing strongly reduces this type of gain with an extremely diagonal transition. This can be quantified by the eigenstates of the lesser Green's function, which represent better states to estimate gain than the conventional eigenstates of the Hamiltonian called Wannier-Stark (WS) states.

The NEGF model allows for a self-consistent evaluation of the transport with respect to both elastic and inelastic scattering as well as interactions with an electromagnetic field in semiconductor heterostructure devices[17–21]. In particular, it is suitable for the study of semiconductor SLs, as it contains simpler approaches, such as miniband transport[1], Wannier-Stark hopping[22,23], or sequential tunneling[24] as limiting cases[25].

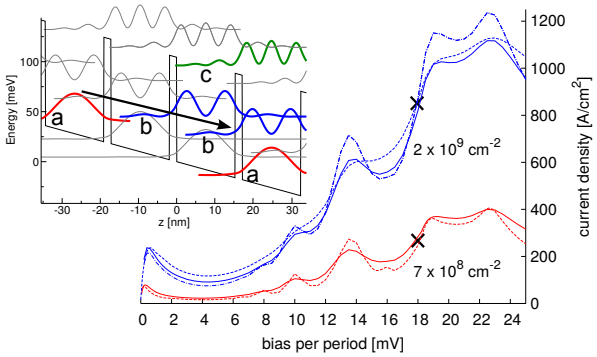

FIG. 1. Current-voltage characteristics for two SLs with different doping densities (full lines). Simulations with modified scattering parameters are displayed as dashed lines, and the one simulation at 40 K is shown as a dotted-dashed blue line. In the inset the configuration of the Wannier states at 18 mV is shown, marked by a cross in the main plot. The gain transition studied is indicated by an arrow.

In NEGF models, scattering is treated by self-energies that are evaluated self-consistently until convergence is reached. These objects are functions of both momentum and energy, but in our implementation they are effectively treated as only energy dependent, and evaluated at a representative set of momentum transfers for the scattering matrix elements[15]. This set is chosen by a typical energy transfer $E_{\mathrm{typ}} = 3\,\mathrm{meV} + 0.5 k_B T$, fitted to give scattering matrix elements matching those calculated with thermalized subbands for other low doped heterostructures. Here, we apply also different values, in order to mimic increased or decreased scattering environments. In this study all samples considered were assumed to be homogeneously doped. Unless stated otherwise, we also keep the lattice temperature fixed at $T = 77$ K, where we consider the model to be both robust and accurate.

FIG. 1 shows the calculated current-voltage characteristics for the device of Ref. 14 (red solid line for a

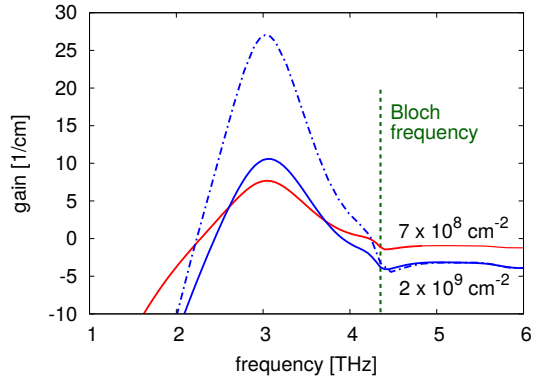

FIG. 2. Simulated gain for the two doping densities studied, both at a bias per period of 18 mV. For the higher doping density, gain at 40 K lattice temperature is also shown (dotted-dashed). There are small signatures of dispersive gain around the Bloch frequency and the structure is mainly transparent at higher frequencies.

doping of $7 \times 10^8/\mathrm{cm}^2$ per period). The peak structure agrees reasonably well with the experimental data shown in FIG. 4 of Ref. 14. For comparison, the experimental shoulder at 19 mV per period, where the ground state is in resonance with the excited state of the 2nd nearest neighbor well, shows a current density of $450\,\mathrm{A/cm}^2$. In the following we focus on the operation point at 18 mV per period, which is a stable operation point with positive differential conductivity. The inset in FIG. 1 shows the Wannier levels at this field. FIG. 2 shows the calculated gain (at weak cavity field). For the nominal structure (red solid line) it remains well below 10/cm, which is probably too small to overcome the total losses.

In the following we will employ a strict naming convention for the SL states (μ, ν) where μ will give the period index, with 0 for the central period, and ν for the state index. Here, Wannier states, are denotes by letters $\nu = a, b, c$ and Wannier-Stark states (WS states, which are the eigenstates of the Hamiltonian) by roman numbers $\nu = i, ii, iii$. The tunneling resonance at the current peak at 19 mV per period is thus between Wannier levels (μ, a) and $(\mu+2, b)$. At 18 mV per period the resonance between these levels is slightly detuned, so that the WS state (μ, i) is dominated by (μ, a) but has significant admixtures from $(\mu+2, b)$ and $(\mu+1, b)$. Similarly, the WS state $(\mu+2, ii)$ is dominated by $(\mu+2, b)$ with significant admixtures from (μ, a), $(\mu+1, b)$, and $(\mu+3, b)$. These states are displayed in FIG. 3 (c) by full lines. The state (μ, i) is lower in energy than $(\mu+2, ii)$ and has thus a significantly larger occupation.

Now the state $(\mu+3, ii)$, which is equivalent to $(\mu+2, ii)$, but shifted to the right and down in energy, is about 14.7 meV below the state (μ, i). As both states extend over several periods they overlap significantly and furthermore there is inversion for the corresponding transition. We can attribute the gain shown in FIG. 2 to this transition, where a slight red shift can be explained by dispersive gain[26].

ρ [1/cm^2]	7×10^8		2×10^9		2×10^9
E_{typ} (meV)	14	6.2	6.2	3.2	4.7 (40 K)
Γ_1(meV)	1.3	2.6	3.4	5.0	2.3 (40 K)
NEGF	19.2	7.30	9.50	-1.64	25.9
FGR(WS)	20.7	11.8	26.6	19.8	37.5
FGR($G^<$)	23.8	8.90	15.4	6.39	29.2

TABLE I. Estimated gain in units cm^{-1} from the gain transition using FGR with WS states and states from diagonalization of the lesser Green's function $G^<$, compared to the full NEGF calculations. In addition the lifetime broadening of the ground state Γ_1 is shown as it has a direct relation to the dephasing strength, as well as the E_{typ} parameter used for each simulation.

As an attempt to improve inversion and gain, the doping was increased to give a sheet density three times higher than the nominal sample. The result on current and gain is shown in FIG. 1 and FIG. 2, respectively. As expected the current density increases approximately by a factor three. However, the peak gain increases only slightly at 77 K. Significantly higher values are found at lower temperatures, where our model suggests gain above 20/cm at 40 K.[27] Furthermore, in both samples there are small signatures of Bloch gain at around 4.2 THz and we also observe that the high doped sample has more dark absorption at frequencies far from the gain transition.

In the following, we want to study, why the increase of gain with doping is limited, so that its practical use appears questionable. A naive guess, would be an increase of gain by a factor three just like the current. However, the inversion might not be proportional to the doping and the linewidth changes with doping. In order to study these effects, we use the standard estimate for the gain using Fermi's Golden Rule (FGR)

$$G(\omega) = \frac{\Delta E_{fi}}{\hbar} \frac{e^2 \Delta n_{fi} z_{fi}^2}{2 n_r c \epsilon_0 d} \frac{\Gamma_w}{(\Delta E_{fi} - \hbar\omega)^2 + \Gamma_w^2/4} \qquad (1)$$

where ΔE_{fi} is the energy difference between the initial and final states, Δn_{fi} is the inversion, z_{fi} the dipole matrix element, n_r is the refractive index and Γ_w is the full width half maximum of the gain peak. These variables can be extracted from the full NEGF model where we diagonalize the Hamiltonian including the real parts of the self-energies, on the diagonal in order to shift the single particle energy levels, to get the WS states. Here we approximate the linewidth as the sum of the lifetimes of the two states involved, $\Gamma_w = \gamma_f + \gamma_i$.

The result of this estimate is shown in TAB. I for a set of different model systems. The second and third column of TAB. I refer to our standard simulation parameters with $E_{\mathrm{typ}} = 6.2$ meV at 77 K, as used in FIGS. 1-2 (full lines). Furthermore, we also performed simulations with altered E_{typ}. The data in the first/fourth column are for decreased/increased scattering compared to their

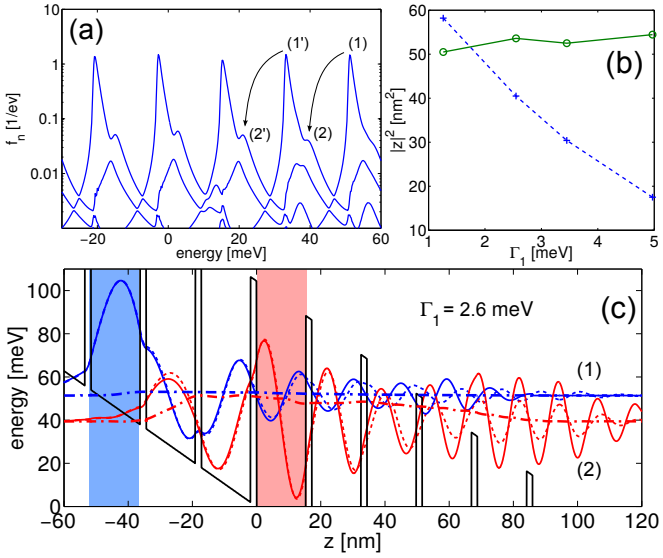

FIG. 3. (a) Eigenvalues $f_n(E)$ of the lesser Green's function $(2\pi\mathrm{i})\, G^<_{\alpha\beta}(\mathbf{k}=0,E)$ at each energy point. (b) Modulus square of the dipole matrix elements against the energy broadening of the ground state. The eigenstates of the density matrix (dashed blue) is strongly dependent on scattering as opposed to WS states (solid green). (c) Real part of the eigenstates (dashed) corresponding to the eigenvalues indicated in (a). The imaginary part is visualized by plotting the current carrying combination[17] $\Re\{-\mathrm{i}\phi^* \mathrm{d}\phi/\mathrm{d}z/m^*\}$ (dotted-dashed) for both eigenstates. These can be seen, especially for state (2), to extend over several periods. For easy comparison we plot also the WS states (μ, i) (blue solid line) and $(\mu+3, ii)$ (red solid line). The well where each wavefunction has its origin is shaded as guidance.

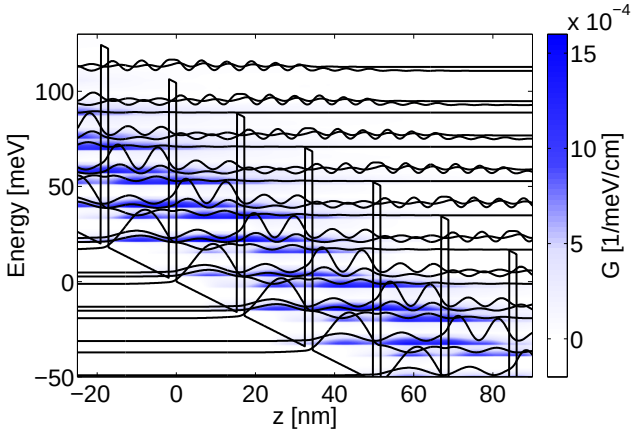

FIG. 4. Gain at 3 THz resolved in energy and space for the nominal case with $\Gamma_1 = 2.6$ meV. The coherence giving rise to the gain extends over several periods. The bias is 18 mV per period.

neighboring column. This is reflected by the respective width of the ground state Γ_1, which is extracted from the NEGF calculation. The current simulations for these parameters are shown by dashed lines in FIG. 1. The minor changes in current can be understood by a slight broadening/sharpening of the tunneling resonances for increased/decreased scattering, respectively. The fifth column in TAB. I gives results for 40 K using our standard temperature dependent E_{typ}.

Let us first consider the estimate from FGR (1) with the common WS states in TAB. I. Here we find, that the peak gain follows essentially the doping density divided by Γ_1, which shows that the inversion is essentially proportional to doping, and all other ingredients, except for the broadening, are constant. In contrast, the NEGF calculation shows a much stronger decrease of gain with Γ_1. While a part of the differences may be attributed to the widening of other absorbing transitions, the large extent is stunning.

To understand this discrepancy we analyze the eigenstates of the lesser Green's function $G^<_{\alpha\beta}(\mathbf{k}, E)$ (which can be viewed as the energetically resolved density matrix) and the corresponding wavefunctions following Ref. 17. The eigenvalues for the nominal case with $\Gamma_1 = 2.6$ are plotted in FIG. 3 (a) for $\mathbf{k} = 0$. The eigenvalues show two sets of peaks, $(\mu, 1)$ and $(\mu, 2)$, corresponding to the ground and excited level. They also visualize the inversion at an energy of 12 meV (indicated by arrows), corresponding to 3 THz. As the eigenvalues are sorted by size in the diagonalization process, we see anti-crossings where the different eigenstates passes each other, so that the state at the eigenvalue indicated by (2) is not the same as the one at (1) since they are separated by at least one anti-crossing.

At the eigenvalue peaks (1) and (2) we plot the corresponding eigenstates in FIG. 3 (c) together with the WS states. From this plot it is possible to see that compared to the WS states, the wavefunction corresponding to the eigenstate $(\mu+3, 2)$ is slightly more localized than the WS state $(\mu+3, ii)$. For these simulation parameters this leads to a decrease of the dipole matrix element. In FIG. 3 (b) the modulus square of the dipole matrix elements are plotted versus the width Γ_1 of the ground state. The WS states show small variations due to mean-field and renormalization due to scattering, but are otherwise constant. In contrast, the dipole matrix elements calculated by the eigenstates of the Green's function, are comparable at low scattering but provide a strong decrease with increasing scattering. These dipole matrix elements can be applied in FGR (1), and the results are given in the lowest line of TAB. I. They actually follow the trend of the full calculation, which demonstrates the relevance of these eigenstates. The result by FGR naturally overestimates the gain slightly, as we consider the gain from only one transition while all other (mostly absorbing) transitions are fully taken into account in the NEGF model.

The strong Γ-dependence of the eigenstates of the lesser Green's function is reflected by dephasing, which affects the coherence length. In this particular situation, the gain is highly diagonal and is thus dependent on

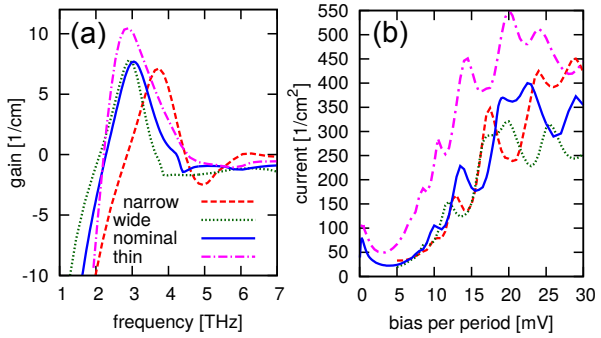

FIG. 5. (a) Gain and current (b) for standard scattering parameters for the three altered structures as well as the nominal sample from Ref. 14. The operating bias per period was 16 mV and 23 mV for the *wide* and *narrow* structure, respectively. For the *thin* structure the bias was fixed at 18.5 mV in the gain simulation.

these spatial coherences. This is further demonstrated in FIG. 4, where the gain stripes extend over more than 50 nm.

As a complement to changing doping, we also tried to optimized the SL by modifying the well and barrier widths. Here we present results for the structures *wide*/*narrow*, where the well is increased/decreased by 4 monolayers, respectively, and the structure *thin*, where the barrier is decreased by 2 monolayers compared to the nominal sample. The sheet doping density was kept constant at $7 \times 10^8/\mathrm{cm}^2$. In FIG. 5 we display gain and current for the samples, which shows that adjusting the well width merely causes a shift in the peak frequency, while thinner barriers improve the performance of the gain medium slightly.

In *conclusion*, we have shown that the NEGF model predicts gain in the structure from Ref. 14. However, the value is below 10/cm at 77 K, which hardly allows for lasing due to waveguide losses. Increasing the doping, lasing at 40 K appears feasible. Further slight optimization by reducing the thickness of the barriers may be possible.

For this highly diagonal transition, the gain is strongly dependent on the scattering. This can be demonstrated by the eigenstates of the lesser Green's function, which essentially differ from the WS states in this case. We demonstrated that these unconventional states are more appropriate to calculate the dipole matrix elements for a quantitative description of gain by Fermi's golden rule.

Acknowledgments: We thank A. Andronov and J. Faist for helpful discussions and the Swedish Research Council for financial support.

* Electronic mail: David.Winge@teorfys.lu.se

1. L. Esaki and R. Tsu, IBM J. Res. Dev. **14**, 61 (1970).
2. S. A. Ktitorov, G. S. Simin, and V. Y. Sindalovskii, Sov. Phys.–Sol. State **13**, 1872 (1972), [Fizika Tverdogo Tela **13**, 2230 (1971)].
3. Y. Shimada, K. Hirakawa, M. Odnoblioudov, and K. A. Chao, Phys. Rev. Lett. **90**, 046806 (2003).
4. P. G. Savvidis, B. Kolasa, G. Lee, and S. J. Allen, Phys. Rev. Lett. **92**, 196802 (2004).
5. N. Sekine and K. Hirakawa, Phys. Rev. Lett. **94**, 057408 (2005).
6. L. Esaki and L. L. Chang, Phys. Rev. Lett. **33**, 495 (1974).
7. H. T. Grahn, ed., *Semiconductor Superlattices, Growth and Electronic Properties* (World Scientific, Singapore, 1995).
8. A. Wacker, Phys. Rep. **357**, 1 (2002).
9. L. L. Bonilla and H. T. Grahn, Reports on Progress in Physics **68**, 577 (2005).
10. A. A. Andronov, E. P. Dodin, D. I. Zinchenko, and Y. N. Nozdrin, Journal of Physics: Conference Series **193**, 012079 (2009).
11. H. Schneider, H. T. Grahn, K. v. Klitzing, and K. Ploog, Phys. Rev. Lett. **65**, 2720 (1990).
12. A. Sibille, J. F. Palmier, and F. Laruelle, Phys. Rev. Lett. **80**, 4506 (1998).
13. M. Helm, W. Hilber, G. Strasser, R. De Meester, F. M. Peeters, and A. Wacker, Phys. Rev. Lett. **82**, 3120 (1999).
14. A. Andronov, E. Dodin, D. Zinchenko, Y. Nozdrin, M. Ladugin, A. Marmalyuk, A. Padalitsa, V. Belyakov, I. Ladenkov, and A. Fefelov, JETP Lett+ **102**, 207 (2015).
15. A. Wacker, M. Lindskog, and D. Winge, Sel. Top. in Quantum Electron., IEEE Journal of **19**, 1200611 (2013).
16. J. Faist, *Quantum Cascade Lasers* (Oxford University Press, Oxford, 2013).
17. S.-C. Lee, F. Banit, M. Woerner, and A. Wacker, Phys. Rev. B **73**, 245320 (2006).
18. T. Schmielau and M. Pereira, Appl. Phys. Lett. **95**, 231111 (2009).
19. T. Kubis, C. Yeh, P. Vogl, A. Benz, G. Fasching, and C. Deutsch, Phys. Rev. B **79**, 195323 (2009).
20. G. Haldaś and, A. Kolek, and I. Tralle, Quantum Electronics, IEEE Journal of **47**, 878 (2011).
21. T. Grange, Phys. Rev. B **92**, 241306 (2015).
22. R. Tsu and G. Döhler, Phys. Rev. B **12**, 680 (1975).
23. D. Calecki, J. F. Palmier, and A. Chomette, J. Phys. C: Solid State Phys. **17**, 5017 (1984).
24. R. F. Kazarinov and R. A. Suris, Sov. Phys. Semicond. **5**, 707 (1971).
25. A. Wacker and A.-P. Jauho, Phys. Rev. Lett. **80**, 369 (1998).
26. R. Terazzi, T. Gresch, M. Giovannini, N. Hoyler, N. Sekine, and J. Faist, Nature Physics **3**, 329 (2007).
27. However, we refrain from making a definite statement on specific values, as our model showed inaccuracies for some quantum cascade lasers at such low temperatures.